Journal of Solid State Electrochemistry (2023) 27:1935–1943
https://doi.org/10.1007/s10008-022-05353-1

ORIGINAL PAPER

Variable work function of semiconducting thin-film oxide electrodes: a case study of SnO_2 and TiO_2

M. Zlamalova[1,2] · V. Mansfeldova[1] · H. Tarabkova[1] · H. Krysova[1] · L. Kavan[1]

Received: 28 October 2022 / Revised: 6 December 2022 / Accepted: 6 December 2022 / Published online: 20 December 2022

Abstract

By atomic layer deposition, we prepared TiO_2 thin films, which do not crack upon thermal treatment at 450–500 °C. The calcination changes the film's work function by tens of meV, as evidenced by electrochemical impedance (Mott-Schottky) and Kelvin probe analyses. In contrast, the work function of ALD-SnO_2 is enhanced by hundreds of meV after this heat treatment. The work function of calcined ALD-SnO_2 films is by ca. 0.3–0.4 eV larger than that of the cassiterite single-crystal electrode. The as-prepared ALD-SnO_2 film exhibits significant anodic photocurrent at potentials, when the calcined film is photoelectrochemically inactive. The ALD growth of SnO_2 on the Au(111) substrate occurs preferentially at the Au grain boundaries. In spite of its non-conformal morphology, the Au-supported SnO_2 film still blocks perfectly the anodic oxidation of ferrocyanide. Electrochemical doping of ALD-SnO_2 by lithium causes a decrease of the work functions by 0.1–0.2 eV in a broad range of film thicknesses.

Keywords Titanium dioxide · Tin dioxide · Mott-Schottky analysis · Flat band potential · Kelvin probe

Introduction

SnO_2 and TiO_2 are top important n-type semiconducting oxides, which have been thoroughly studied in the past [1–3]. The work function and conduction band minimum of these oxides represent salient characteristics for understanding their electrochemistry, and for the development of applications, e.g., in energy conversion and storage [1–5]. Yet, the available data are often inconsistent, which provoked conflicting debate in the past [6]. We have recently addressed this problem by a comparative study of well-defined TiO_2 single crystals, and found that the differences in the work functions can be as high as ≈1 eV, if they are measured by the three standard techniques, i.e., ultraviolet photoelectron spectroscopy (UPS), Kelvin probe, and electrochemical impedance spectroscopy (determination of flat band potential by the Mott-Schottky analysis) [6]. These changes are mainly ascribed to different environments of the investigated surface. Indeed, the *operando*-photoelectron spectroscopy of the TiO_2 surface under electrochemical control provided an identical value of flat band potential as the Mott-Schottky plot [7].

A recent review by Patel et al. [2] pointed out that the flat band potentials were sometimes measured incorrectly and on inappropriate materials, e.g., on nano-porous electrodes. The single-crystal electrodes are ideal for fundamental studies, but practical applications rely on polycrystalline (nanocrystalline) materials. They are frequently deposited in thin films on transparent conducting substrates, such as F:SnO_2 (FTO), and subjected to subsequent thermal annealing for applications, e.g., in dye-sensitized and perovskite solar cells [1, 3–5, 8–10]. Characterization of these films by flat band potentials is challenging, sometimes even impossible for fundamental reasons [2]. On the other hand, the compact nm-thin films can ultimately mimic the behavior of single-crystal electrodes by empowering the creation of space-charge layer and band-bending in contact with the electrolyte solution. A basic condition is that the films must not contain pinholes accessible for the electrolyte solution [2]. Atomic layer deposition (ALD) is a versatile technique to grow high-quality dense films, and the measurement of flat band potentials on TiO_2 [11–13] and SnO_2 [14, 15] thin

✉ L. Kavan
kavan@jh-inst.cas.cz

[1] J. Heyrovsky Institute of Physical Chemistry, CAS, Dolejskova 3, 18223 Prague 8, Czech Republic

[2] Department of Inorganic Chemistry, Faculty of Science, Charles University, Hlavova 2030, 128 40 Prague, Czech Republic

films on the FTO substrates provided reasonably consistent data.

The as-grown ALD-TiO_2 was quasi-amorphous, but crystallized to anatase upon heat treatment at 500 °C [11]. Unfortunately, this treatment is accompanied by cracking of titania thin films [12], which essentially precludes the determination of flat band potential (V_{FB}) in the calcined films as discussed above. Interestingly, the ALD-made SnO_2 thin films were found to be stable against thermal cracking, and this allowed the measurement of flat band potential even for the heat-treated nm-thin SnO_2 films [14, 15]. They were again quasi-amorphous at the usual deposition temperatures (below ca. 150 °C) [5, 16, 17], but tetragonal rutile phase was detected by X-ray diffraction at higher deposition temperatures [16–18]. The tip-enhanced Raman spectroscopy confirmed better crystallinity for post-annealed SnO_2 films, too [8].

Our previous electrochemical study of ALD-SnO_2 revealed a large upshift of the V_{FB} for calcined SnO_2: by ca. 0.5 V in films which were treated at 450 °C as referenced to the V_{FB} value of the as-prepared (amorphous) film [14]. This observation was qualitatively confirmed by a follow-up UPS study by Lee et al. [8] reporting on the 0.35 eV enhancement of the work function (φ) in the ALD-SnO_2 calcined at 300 °C. If we do not consider the effect of different environments surrounding the investigated surface (electrolyte solution or vacuum) [6], the work function is simply related to V_{FB}:

$$\varphi = -eV_0^{SHE} + eV_{FB} \quad (1)$$

where e is the electron charge; V_0^{SHE} is the potential of the standard hydrogen electrode (SHE) in the absolute scale; $V_0^{SHE} \approx -4.44$ V [19]. V_{FB} is quoted at pH corresponding to the isoelectric point of the electrode material, and is expressed in the SHE scale [6]. The isoelectric point was reported to be 7.9 for ALD-TiO_2 and 8.2 for ALD-SnO_2 [20]. (We may note that these values are quite different from those reported in earlier literature, particularly for SnO_2.) In addition to thermal calcination, which significantly enhanced the V_{FB} and φ values of SnO_2, a small decrease (by about 0.15 V and 0.1 eV, respectively) was observed for ALD-SnO_2 thin films, which were subjected to electrochemical doping with Li in an aprotic medium [15]. The electrochemical doping was ascribed to a substitution of Sn^{4+} by Li^+ [15]. This reaction is obviously excluded with TiO_2, in which Li is accommodated by insertion, causing even structural changes in the crystal lattice [21].

The quasi-amorphous ALD-TiO_2 thin films exhibited their V_{FB} values typically in the range from ca. − 0.1 V to 0.1 V vs RHE (reversible hydrogen electrode) [2, 11, 12], which is nearly identical to the corresponding values found for crystalline anatase thin films and even for the anatase single crystal (− 0.16 to − 0.1 V vs. RHE) [2, 6]. To the best of our knowledge, the striking difference between the thermal sensitivity of quasi-amorphous SnO_2 and TiO_2 was not yet satisfactorily explained. (Quite surprisingly, there are almost no data for V_{FB} of SnO_2 single-crystal electrodes [2] which would allow analogous comparison of quasi-amorphous and crystalline SnO_2.) Furthermore, a recent study of vacuum-evaporated tin oxide films revealed just the opposite effect of thermal treatment (180–200 °C): a *decrease* of V_{FB} in the calcined films [10], rather than an *increase* which was reported for ALD-SnO_2 [8, 9, 14, 15]. Eventually, the high sensitivity of ALD-TiO_2 to thermal cracking [12] is yet another complication of the measurement of the V_{FB} upon calcination. All these open questions ask for new studies and for extended materials' characterization by several independent methods to account for the alternations caused by the environment effects [6].

Experimental section

Materials and electrodes

FTO glass (NSG10, Nippon Sheet Glass, 10 Ohm/sq) was cleaned ultrasonically using deionized water, acetone, isopropyl alcohol, and ethanol for 10 min in each solvent. The Au(111) substrates (11 × 11 mm^2, 250 nm Au, 2.5 nm Cr intermediate layer on borosilicate glass, Arrandee) were fabricated by flame annealing and cooled down in an argon atmosphere. The TiO_2 and SnO_2 films were prepared by thermal-mode ALD in the R-200 standard reactor (Picosun, Finland). The TiO_2 films were prepared using tetrakis(dimethylamido)titanium(IV) (TDMATi from Strem Chemicals) and water (EpiValence). The TDMATi was evaporated at 85 °C. The substrate temperature was 150 °C (in some cases also 200 °C) and the pressure was 1000 Pa during the deposition. One TiO_2 deposition cycle comprised of pulse-purge sequence: 1.6 s TDMATi – 6 s N_2 – 0.1 s H_2O – 8 s N_2. The SnO_2 films were fabricated by alternating pulses of tetrakis(dimethylamido)tin(IV) (TDMASn from Strem Chemicals) and water. The evaporation temperature for TDMASn was 65 °C. The substrate temperature was 118 °C and the pressure was 700 Pa during the deposition. One SnO_2 deposition cycle consisted of 1.6 s TDMASn pulse time, 6 s N_2 gas purge, 0.1 s H_2O pulse time, and 9 s N_2 purge. The growth rate was 0.141 nm/cycle (for TiO_2) and 0.061 nm/cycle (for SnO_2); calibrated by ellipsometry (EP4, Accurion). Nitrogen (Messer Technogas, 99.999%) was used as the carrying and purging gas. For post-annealing, the as-prepared films were calcined for 1 h in the air at the given temperature (450 °C or 500 °C); the heating ramp was 5 °C/min. The naturally doped, black SnO_2 single crystal (5 × 5 × 0.5 mm^3;

cassiterite (001) orientation) was purchased from SurfaceNet, GmbH (Germany). It was contacted by Ga-In alloy to a Cu wire, and sealed using TorrSeal epoxy (Varian).

Characterization methods

Kelvin probe measurements (macroscopic variant) were carried out using the KP020 instrument (KP Technology Ltd). The gold probe was positioned close to the sample surface and the contact potential difference was measured. The electrical connection to the sample surface was realized by using an indium tape. Work functions were calibrated using a freshly peeled-off highly oriented pyrolytic graphite; its work function was set to 4.6 eV [22]. Peak force Kelvin probe force microscopy (KPFM) was studied using the peak force Kelvin probe, Dimension Icon (Bruker, USA) with the SCM-PIT-V2 tip. The contact potentials were calibrated by gold using the Al/Si/Au PFKPFM-SMPL standard (Bruker); the work function of Au was set to 5.1 eV [23]. Tapping mode atomic force microscopy (AFM) images were obtained using Dimension Icon microscope with silicon cantilever VTESPA-300 (resonant frequency $f_{res} \approx 300$ kHz, spring constant $k = 42$ N·m^{-1}, nominal tip radius 5 nm, Bruker, USA).

Electrochemical measurements

Electrochemical measurements were carried out with Autolab 302 N apparatus (Metrohm) equipped with a frequency response analyzer (FRA). The counter-electrode was a platinum wire (or Pt mesh for impedance measurements) and the reference electrode was Ag/AgCl (sat. KCl). The electrolyte solution was 0.5 M KCl; its pH was adjusted by HCl. Alternatively, the electrolyte solution was also 0.1 M lithium bis(trifluoromethylsulfonyl)imde (LiTFSI) in acetonitrile. In this case, the reference electrode was non-aqueous Ag/AgCl (sat. LiCl in ethanol) which was interfaced by a bridge with 0.1 M LiTFSI. Its potential was calibrated using ferrocene (200 µL of 0.1 M acetonitrile solution per 10 mL of electrolyte solution added and tested using the Pt working electrode). The electrolyte solution was purged with Ar, and the measurement was carried out under Ar in a closed electrochemical cell.

Electrochemical impedance spectroscopy (EIS) was investigated in the frequency range from 100 kHz to 0.1 Hz (modulation amplitude 10 mV) at varying potentials. Spectra were evaluated using Zview (Scribner) software by fitting to a Randles-type circuit. Here, R_{CT} is the charge-transfer resistance, which is parallel to the constant phase element (*CPE*) to account for non-ideal capacitive behavior [6, 11, 12, 14, 24]. Electrochemical impedance spectra were evaluated using ZView (Scribner) software by fitting to a standard Randles-type equivalent circuit as in [6]. The circuit is composed of the charge-transfer resistance (R_{CT}), which is parallel to the constant phase element (*CPE*). The circuit further contains a series resistance, R_S, characterizing the ohmic resistance of electrodes, electrical contacts, and electrolyte solution, and the Warburg impedance, Z_W corresponding to the ionic transport in solution. The impedance of *CPE* equals [24]:

$$Z_{CPE} = B^{-1}(i\omega)^{-\beta} \tag{2}$$

with ω being the EIS circular frequency; B (admittance pre-factor) and β (exponent) are the frequency-independent parameters of the CPE ($0.8 \le \beta \le 1$; experimental values were from 0.8 to 0.9). The interfacial capacitance, C, is calculated from [24]:

$$C = \frac{(R_{CT} \cdot B)^{1/\beta}}{R_{CT}} \tag{3}$$

The source data (R_{CT}, B, and β) were determined by fitting the complete impedance spectra (measured at each applied potential from 100 kHz to 0.1 Hz). This obviously removes the problem of "frequency dispersion" of the Mott-Schottky plots [12].

Photoelectrochemical measurements were performed in an Ar-saturated 0.1 M Na_2SO_4 solution (pH 10; adjusted by 0.1 M NaOH) and the cell was equipped with a fused silica optical window. The photoelectrochemical cell was placed in a dark room and controlled by the Zahner workstation. The films were illuminated from the front side by the UV LED diode (LS365-2) intensity of 100 W/m^2. The photoexcitation was applied with 5 s dark/light intervals. During this test, the pH of the electrolyte solution was unchanged within the experimental error (± 0.05 pH). The passed charge of water oxidation was of the order of 1 mC, which translates into ca. 10^{-8} mol of H^+. This amount of photogenerated protons is then smoothly neutralized by the electrolyte solution of pH 10.

Electrolytes, solvents, and other chemicals were of the standard quality (p.a. or electrochemical grade) purchased from Aldrich or Merck. LiTFSI was dried at 200 °C in a vacuum and subsequently handled in a glove box under Ar. Acetonitrile (99.8%, anhydrous) was further dried by a 4A molecular sieve.

Results and discussion

As discussed above, the preparation of dense TiO_2 films by post-annealing of quasi-amorphous ALD-TiO_2 (1–6 nm in thickness) failed due to the thermal cracking [12]. The film damage can be quantified by electrochemical tests with suitable redox probes, such as $[Fe(CN)_6]^{3-/4-}$, which selectively distinguish the charge-transfer reactions occurring on the

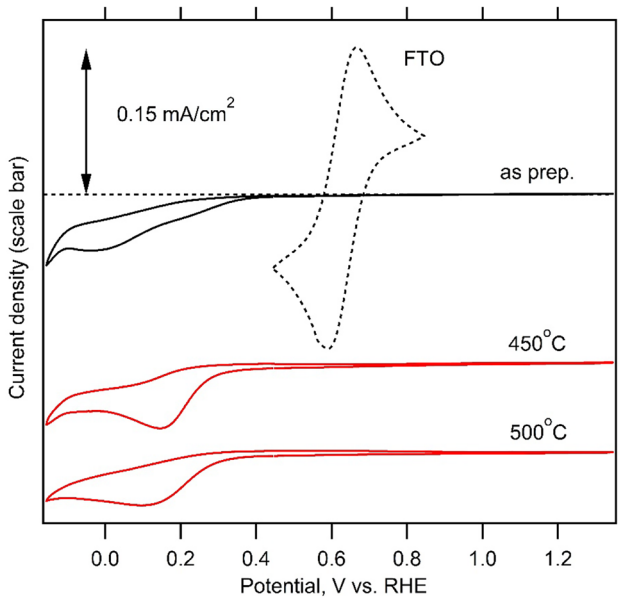

Fig. 1 Cyclic voltammogram of a bare FTO electrode (dashed line) and that covered by ALD-TiO_2 thin film; 22 nm in thickness (black line: as-prepared; red lines: calcined at 450 °C and 500 °C, respectively). Scan rate 50 mV/s. Electrolyte solution is 0.5 mM $K_4Fe(CN)_6$ + 0.5 mM $K_3Fe(CN)_6$ in aqueous 0.5 M KCl, pH 2.5. The voltammograms of calcined samples are offset for clarity, but the current density scale is the same for all voltammograms

TiO_2 surface and on the supporting FTO in the denuded areas of the film [12].

By screening of experimental conditions, we found that the pinhole-free and thermally unperturbed films can be grown simply by enhancement of the TiO_2 film thickness. Figure 1 shows an example of the 22-nm-thick TiO_2 film exhibiting perfect blocking even after its calcination at 450–500 °C in air. To the best of our knowledge, this is the first demonstration that dense amorphous ALD-TiO_2 film can survive the thermal crystallization without cracking.

The onset potential of ferricyanide reduction during cyclic voltammetry is similar for all our TiO_2 films, independent of the post-calcination (Fig. 1). This potential is known to scale with the flat band potential of the electrode material [10]; hence, cyclic voltammetry evidences that the V_{FB} is nearly intact by heat treatment.

The Mott-Schottky plots provide a more accurate analysis of the V_{FB} change upon thermal treatment (Fig. 2). The found V_{FB} equals − 0.08 V vs. RHE for the as-prepared quasi-amorphous ALD-TiO_2. It only slightly increases to 0.0 V vs. RHE for the same material after calcination at 450 °C. Our finding essentially matches the work of Hoffeditz et al. [13] reporting on small changes of V_{FB} caused by calcination (0.008 V decrease), but thermal cracking of the film was not tested in the cited work. The doping density (N_D) from the slope of the Mott-Schottky plot is 2.1 • 10^{20} cm^{-3} and 3.7 • 10^{20} cm^{-3} for our pristine and calcined film, respectively (Fig. 2). These values are comparable to the donor densities reported by others [11, 12] (but we need to admit that they actually just upper estimates assuming the projected area of electrodes).

The width of space-charge layer (W) can be determined from the equation:

$$W = \left(\frac{2\varepsilon_0\varepsilon_r}{eN_D}\right)^{1/2}\left(V - V_{FB} - \frac{k_BT}{e}\right)^{1/2} \quad (4)$$

ε_0 is the permittivity of free space, ε_r is the dielectric constant ($\varepsilon_r \approx 55$ for TiO_2 anatase) [12], e is the electron charge, k_B is the Boltzmann constant, and T is temperature. Equation (4) predicts (for the 1 V band-bending and the experimentally found N_D values) the width W of 5 nm and 4 nm for our pristine and calcined films, respectively. Hence, the used TiO_2 film thickness (22 nm) is sufficient to accommodate the depletion layer, without its penetrating into the supporting FTO, which occurs for thinner films [12]. Yet, the main conclusion from our analysis is that the strong enhancement

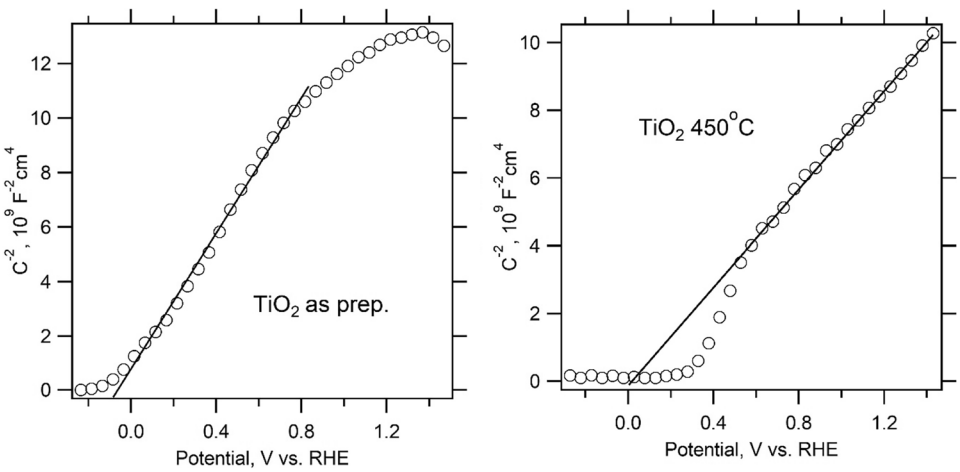

Fig. 2 The Mott-Schottky plot for ALD-TiO_2 thin film, 22 nm in thickness. Left chart: as-prepared film; right chart: the same film after calcination at 450 °C. The electrolyte solution is aqueous at 0.5 M KCl, pH 4. Potentials were measured with Ag/AgCl reference electrode but are recalculated against RHE

of V_{FB} caused by thermal crystallization (which occurs for the ALD-SnO_2 thin films [14]) is not replicated for TiO_2.

Kelvin probe measurement on the same film (22 nm TiO_2) provided the work functions of 4.22 eV, 4.22 eV, and 4.21 eV for the as-prepared film, calcined at 450 °C and calcined at 500 °C, respectively. (Additional data are collected in Table S1, Supporting Info.) The found values are not too far from the work function reported for the Kelvin probe measurement on anatase (101) single crystal, 4.40 eV [6]. This confirms that the thermal treatment and/or crystallization of ALD-TiO_2 has a small effect on its work function, which is in sharp contrast to ALD-SnO_2.

To get further insight into these differences, we have investigated the photoelectrochemical current/voltage plots under intermittent irradiation by UV light (Fig. 3). Our comparison of TiO_2 and SnO_2 illustrates the principal differences in the photoelectrochemical activity of quasi-amorphous and calcined films. In terms of the classical Gärtner-Butler model, the onset of anodic photocurrent theoretically coincides with the V_{FB}. This is nearly fulfilled for crystalline TiO_2, but ALD-TiO_2 films exhibit significant overpotential (≈0.4 V) for the photocurrent generation [2]. The behavior of SnO_2 is qualitatively different: Fig. 3 (right chart) shows that anodic photocurrent flows on quasi-amorphous SnO_2 even at potentials, when the calcined film is still photoelectrochemically inactive. Also, the onset potential of cathodic dark current, which is another measure of switching from the depletion to accumulation regime of the semiconductor [25], exhibits the same trends for SnO_2 and TiO_2: this potential is more positive for the calcined vs. the as-prepared SnO_2. On the other hand, TiO_2 shows negligible or slightly opposite changes (Fig. 3 left chart) after calcination.

Figure 4 shows the Mott-Schottky plot for the commercial SnO_2 single crystal; cassiterite (001) orientation. The analysis gives $V_{FB} = 0.41$ V vs. RHE and $N_D = 1.3 \cdot 10^{20}$ cm^{-3}. There are surprisingly few earlier studies of the V_{FB} on SnO_2 single crystal [2]. The classical paper by Bolts and Wrighton

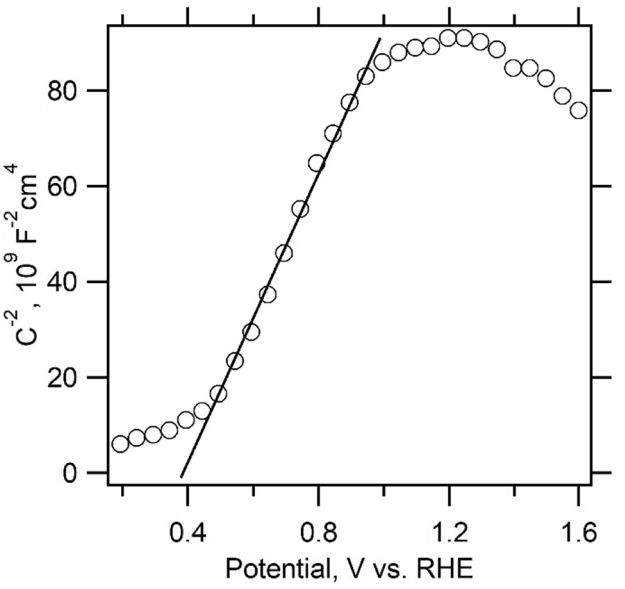

Fig. 4 The Mott-Schottky plot for SnO_2 single-crystal cassiterite electrode, (001) orientation. The electrolyte solution is aqueous 0.5 M KCl, pH 4. Potentials are measured with Ag/AgCl reference electrode but are recalculated against RHE

[26] reported a value of 0.31 V vs. RHE. The second paper by King et al. [27] quoted 0.44 and 0.56 V vs. RHE for SnO_2 single crystals in the (100) and (111) orientations, respectively. In the first case, the Mott-Schottky measurement was made at a single frequency only [26]. In the second case, this experimental detail is unknown, and furthermore, there seems to be some inconsistency between the text and pictures in [27] (the value of 0.56 V appears to be overestimated by ca. 0.1 V).

In spite of these small deficiencies, the literature data for SnO_2 single crystal are still roughly comparable to our value ($V_{FB} = 0.41$ V, Fig. 4). This finding, however, raises a general question about the thermal crystallization of ALD-SnO_2

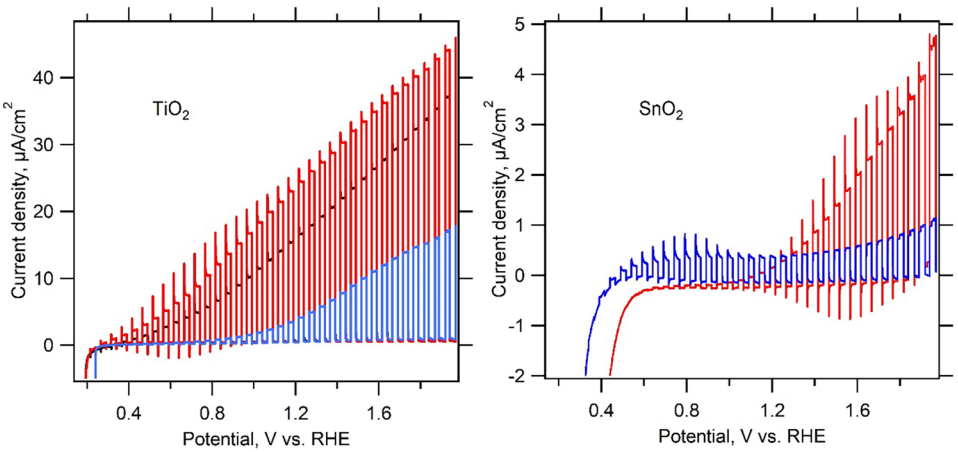

Fig. 3 Linear sweep voltammetry under intermittent UV light. The photoexcitation was applied with 5 s dark/light intervals. Electrolyte solution is aqueous 0.1 M Na_2SO_4, pH 10. Left chart: ALD-TiO_2 film, thickness 22 nm, blue line: as-prepared; red line: calcined at 450 °C, black line: calcined at 500 °C. Right chart: ALD-SnO_2 film, thickness 22 nm, blue line: as-prepared; red line: calcined at 450 °C

films. The latter exhibit the V_{FB} of 0.2 V vs. RHE for the as-received films, and 0.7 V vs. RHE for the same films after calcination at 450 °C [14]. In other words, the thermal crystallization of ALD-SnO_2 provides a material with significantly more positive V_{FB} than that of the SnO_2 single crystal (by ca. 0.3 V).

To verify this unexpected finding, we investigated the work function independently by Kelvin probe measurements. Figure 5 shows the data for ALD-SnO_2 deposited at the FTO substrate for varying film thicknesses between 5 and 120 nm. Our values for the as-prepared quasi-amorphous films are comparable to the work function reported by Baena et al. [28] from UPS (4.46 eV for the 15-nm film) but somewhat larger than the values of 4.15–4.18 eV reported by others from similar experiments [8, 16]. More importantly, we observe a ca. 0.5 eV increase of the work function, if the as-prepared film is calcined at 450 °C. The corresponding work functions determined from the V_{FB} values [14] and Eq. (1) equal 4.2 eV and 4.7 eV for the as-prepared and calcined SnO_2 thin-film, respectively. (The same evaluation routine gives the work function of 4.4 eV for our SnO_2 (001) cassiterite single-crystal electrode, cf. Figure 4.)

The Kelvin probe measurements of our SnO_2 single crystal provided the work function of 4.48 eV. For the sake of swift comparison, this value is shown in Fig. 5, too. It is quite close to the work function calculated from the electrochemical data (4.4 eV); see the previous paragraph. More importantly, our Kelvin probe measurements confirm that the thermal treatment of ALD-SnO_2 provides a material with a significantly larger work function (by ca. 0.4 eV) than that of a cassiterite single crystal. Hence, there must be some other mechanisms (beyond simple crystallization) which cause such a dramatic enhancement of the work function of the calcined ALD-SnO_2. The explanation is still unclear, but Aygüler et al. [5] discussed the influence of deep trap states below the Fermi level, which are attributed to defects, e.g., oxygen vacancies in SnO_2. Another cause of defect states could be hydrogen impurities incorporated during ALD growth [16]. The defect formation (and the electronic structure near the Fermi level) depend in a complex way on deposition temperature, substrate, oxidant agent (H_2O, O_2, or O_3), and ALD growth mode (thermal or plasma enhanced) [16, 29]. Details are collected in Table S3 (Supporting Info).

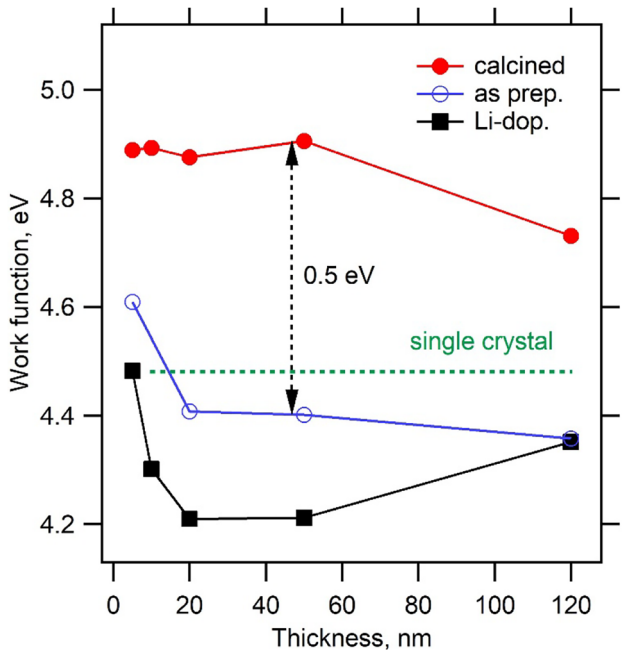

Fig. 5 Work functions determined by Kelvin probe measurement for SnO_2 films of varying thicknesses deposited on FTO. Blue circles are for the as-prepared (quasi-amorphous) films. Red circles are for the same films calcined at 450 °C in air. Black squares are for the same films after electrochemical doping with Li. The lines connecting experimental points are guides for the eyes. The green dashed line indicates the value of the work function determined by the Kelvin probe measurement of cassiterite (001) single-crystal

Our finding qualitatively agrees with the recent work of Erdenebileg et al. [30] reporting on a strong downshift of the conduction band minimum of ALD-SnO_2 deposited at various temperatures: their UPS study indicated a downshift of 0.66 eV for the film deposited at 200 °C as compared to the film deposited at 80 °C. In a similar work, Kuang et al. [17] reported a downshift of 0.62 eV for films deposited at 200 °C as referenced to films grown at 50 °C. On the other hand, these data on ALD-SnO_2 sharply contrast the changes of V_{FB} in vacuum-evaporated SnO_x thin films [10]: in this case, the V_{FB} dropped by ca. 0.25 V for film annealed at 180 and 200 °C. We have no simple explanation for this paradox (it was not discussed in the cited work), but we should note that the vacuum-evaporated films contain some amount of Sn(II) impurities, perhaps SnO [10].

We further investigated the SnO_2 films, which were subjected to electrochemical doping by Li. To this purpose, the SnO_2 films were grown by ALD either on FTO or Au(111) substrates. The as-received films were subsequently treated in the solution of 0.1 M LiTFSI + acetonitrile following the procedure described in [15]. Figure 5 summarizes the data for our FTO-supported films. The doping causes the drop of work functions by ca. 0.1–0.2 eV in a broad range of the film thicknesses, except for the thickest film (120 nm) which we shall not discuss at this point. The drop of φ values observed for thin films by Kelvin probe measurements is in good accord with the changes found by photoelectron spectroscopy and electrochemistry [15]. The actual drop of φ values is in the same range (from 0.1 to 0.2 eV) for all the used three standard techniques. Detailed data are collected in Table S2 (Supporting Info).

Figure S1 (Supporting Info) presents the work functions of SnO_2, which were determined by peak force Kelvin probe force microscopy (KPFM) on the Au(111) substrate. For

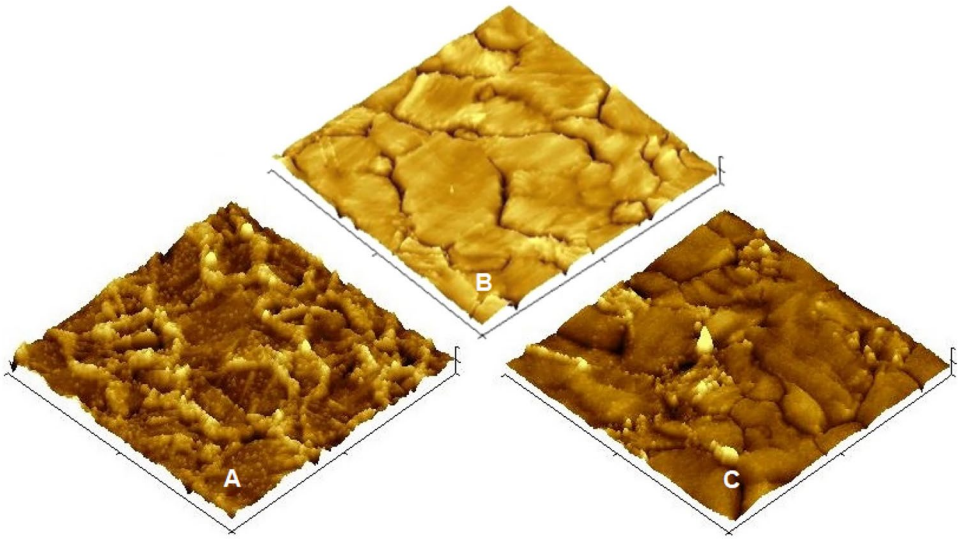

Fig. 6 AFM taping-mode height (3D) images (5×5 μm^2) of the 120-nm-thick ALD-SnO_2 film deposited on Au(111) substrate. **A** As-prepared film; **C** the same film after calcination at 450 °C. The bare Au(111) substrate is shown in chart **B**. The vertical scale range is 60 nm for all plots

comparison, Fig. S1 also shows the corresponding data from the standard macroscopic Kelvin probe (KP) measurements of the same samples. The effect of calcination is still obvious, but KPFM almost does not distinguish the effect of Li doping. We ascribe this observation to the fact that in KPFM, the tip interacts with the surface closely, and thus the probe properties can be changed by contamination with material from the sample. The Li doping is known to affect the film down to several nm underneath the surface only [15].

The second reason for perturbation of the work functions measured on Au(111) substrates consists in the fact that the ALD deposition of SnO_2 Au(111) is inhomogeneous. This is documented by AFM images shown in Fig. 6 (additional data are presented in Fig. S2, Supporting Info). The as-prepared SnO_2 films on Au(111) show preferable deposition at the Au grain boundaries, which is particularly expressed for thicker SnO_2 layers (Figs. 6 and S3). Interestingly, these irregular films still exhibit good blocking function, probed by the standard ferri-/ferrocyanide test (Fig. S5, Supporting Info). Calcination at 450 °C causes smoothing of these irregularities in addition to the crystallization-driven coarsening of the SnO_2 film which is seen at the flat areas of Au(111) substrate (Fig. S3). This effect was previously investigated by SEM and TEM microscopy on FTO-supported SnO_2 films [14].

Due to the larger roughness of the bare FTO substrate, AFM does not distinguish the nanomorphology of thin SnO_2 film from the structure of the FTO substrate. There are no significant differences between the roughness and nanomorphology of the bare FTO substrate, evidencing that SnO_2 coverage is conformal (Fig. S3, S6). (The conformal morphology of ALD-SnO_2 on FTO is directly seen by cross-sectional SEM images reported by others [8, 9, 17, 28].)The differences in deposition mechanism can explain variations of Kelvin probe data for SnO_2 films deposited on different substrates. More specifically, the work functions measured on Au-supported films are, in general, less reliable due to the complicated film morphology. The high-resolution AFM images (Fig. S4) do not show any significant differences in the nanomorphology of the bare and Li-doped SnO_2 film deposited on Au(111).

Conclusions

The 22-nm-thick TiO_2 thin film grown by ALD on the FTO substrate does not crack upon thermal treatment at 450–500 °C in the air (like thinner films; 1–6 nm). This is evidenced by blocking the ferrocyanide oxidation. Such a thermally stable TiO_2 film is suitable for the investigation of the changes of flat band potentials (work functions) during the transformation from quasi-amorphous to crystalline (anatase) form. The variations are of the order of tens of meV, as indicated by EIS (Mott-Schottky) and Kelvin probe analyses. The found values for ALD-TiO_2 films are even comparable to those for the TiO_2 (anatase) single crystal. Hence, the transformation of quasi-amorphous TiO_2 to crystalline anatase has only a small effect on the work function.

In sharp contrast to the behavior of TiO_2, the ALD-SnO_2 exhibits a dramatic enhancement of the work function, by hundreds of meV (typically 0.5 eV) as a result of calcination. This is confirmed by all the standard techniques, i.e., by EIS, photoelectron spectroscopy, Kelvin probe, and KPFM. The photoelectrochemical current/voltage plots under intermittent irradiation by UV light provide yet another demonstration of the differences in work functions: the quasi-amorphous SnO_2 exhibits significant anodic photocurrent at potentials, when the calcined film is still photoelectrochemically inactive. The thermal treatment of ALD-SnO_2 provides a material with a significantly larger work function than that

of a cassiterite single-crystal electrode (001)-orientation (by ca. 0.3–0.4 eV).

The high-resolution AFM imaging requires flat substrates, such as flame-annealed Au(111). However, the ALD growth of SnO_2 on gold is not conformal. Though the film is still well blocking the ferrocyanide oxidation, the taping-mode AFM images evidence preferential deposition at the Au grain boundaries. Consequently, the work function measurements of ALD films are less reliable on the Au(111) substrate compared to the FTO substrate.

Electrochemical doping of ALD-SnO_2 by lithium causes a drop of work functions by ca. 0.1–0.2 eV as evidenced by EIS and Kelvin probe measurements in a broad range of the film thicknesses, but no obvious changes of the surface nanomorphology. In summary, the ALD-SnO_2 film represents a unique material, whose work function can be tuned in the range of ca. 0.7 eV simply by doping or calcination. This behavior is not replicated for the ALD-TiO_2 films.

Supplementary Information The online version contains supplementary material available at https://doi.org/10.1007/s10008-022-05353-1.

Funding This work was supported by the Grant Agency of the Czech Republic (contract No. 22-24138S).

Declarations

Competing interests The authors declare no competing interests.

References

1. Kavan L (2019) Conduction band engineering in semiconducting oxides (TiO_2, SnO_2): applications in perovskite photovoltaics and beyond. Catal Today 328:50–56
2. Patel MY, Mortelliti MJ, Dempsey JL (2022) A compendium and meta-analysis of flatband potentials for TiO_2, ZnO, and SnO_2 semiconductors in aqueous media. Chem Phys Rev 3:011303
3. Park SY, Zhu K (2022) Advances in SnO_2 for efficient and stable n-i-p perovskite solar cells. Adv Mater 34:e2110438
4. Kim M, Jeong J, Lu H, Lee TK, Eickemeyer FT, Liu Y, Choi IW, Choi SJ, Jo Y, Kim HB, Mo SI, Kim YK, Lee H, An NG, Cho S, Tress WR, Zakeeruddin SM, Hagfeldt A, Kim JY, Grätzel M, Kim DS (2022) Conformal quantum dot- SnO_2 layers as electron transporters for efficient perovskite solar cells. Science 375:302–306
5. Ayguler MF, Hufnagel AG, Rieder P, Wussler M, Jaegermann W, Bein T, Dyakonov V, Petrus ML, Baumann A, Docampo P (2018) Influence of Fermi level alignment with tin oxide on the hysteresis of perovskite solar cells. ACS Appl Mat Interfaces 10:11414–11419
6. Mansfeldova V, Zlamalova M, Tarabkova H, Janda P, Vorokhta M, Piliai L, Kavan L (2021) Work function of TiO_2, (anatase, rutile, and brookite) single crystals: effects of the environment. J Phys Chem C 125:1902–1912
7. Lichterman MF, Hu S, Richter MH, Crumlin EJ, Axnanda S, Favaro M, Drisdell W, Hussain Z, Mayer T, Brunschwig BS, Lewis NS, Liu Z, Lewerenz HJ (2015) Direct observation of the energetics at a semiconductor/liquid junction by operando X-ray photoelectron spectroscopy. Energy Environ Sci 8:2409–2416
8. Lee Y, Lee S, Seo G, Paek S, Cho KT, Huckaba AJ, Calizzi M, Choi DW, Park JS, Lee D, Lee HJ, Asiri AM, Nazeeruddin MK (2018) Efficient planar perovskite solar cells using passivated tin oxide as an electron transport layer. Adv Sci 5:1800130
9. Jeong S, Seo S, Park H, Shin H (2019) Atomic layer deposition of a SnO_2 electron-transporting layer for planar perovskite solar cells with a power conversion efficiency of 18.3%. Chem Commun 55:2433–2436
10. Kodur M, Dorfman Z, Kerner RA, Skaggs JH, Kim T, Dunfield SP, Palmstrom A, Berry JJ, Fenning DP (2022) Electrochemical screening of contact layers for metal halide perovskites. ACS Energy Lett 7:683–689
11. Moehl T, Suh J, Severy L, Wick-Joliat R, Tilley SD (2017) Investigation of (leaky) ALD TiO_2, protection layers for water-splitting photoelectrodes. ACS Appl Mat Interfaces 9:43614–43622
12. Kavan L, Tetreault N, Moehl T, Grätzel M (2014) Electrochemical characterization of TiO_2, blocking layers for dye sensitized solar cells. J Phys Chem C 118:16408–16418
13. Hoffeditz WL, Pellin MJ, Farha OK, Hupp JT (2017) Determining the conduction band-edge potential of solar-cell-relevant Nb_2O_5 fabricated by atomic layer deposition. Langmuir 33:9298–9306
14. Kavan L, Steier L, Grätzel M (2017) Ultrathin buffer layers of SnO_2 by atomic layer deposition: perfect blocking function and thermal stability. J Phys Chem C 121:342–350
15. Kavan L, Vlckova-Zivcova Z, Zlamalova M, Zakeeruddin SM, Grätzel M (2020) Electron-selective layers for dye-sensitized solar cells based on TiO_2 and SnO_2. J Phys Chem C 124:6512–6521
16. Martínez-Puente MA, Tirado J, Jaramillo F, Garza-Hernández R, Horley P, Silva Vidaurri LG, Aguirre-Tostado FS, Martínez-Guerra E (2021) Unintentional hydrogen incorporation into the SnO_2 electron transport layer by ALD and its effect on the electronic band structure. ACS Appl Energy Mater 4:10896–10908
17. Kuang Y, Zardetto V, van Gils R, Karwal S, Koushik D, Verheijen MA, Black LE, Weijtens C, Veenstra S, Andriessen R, Kessels WMM, Creatore M (2018) Low-temperature plasma-assisted atomic-layer-deposited SnO_2 as an electron transport layer in planar perovskite solar cells. ACS Appl Mater Interfaces 10:30367–30378
18. Choi DW, Maeng WJ, Park JS (2014) The conducting tin oxide thin films deposited via atomic layer deposition using tetrakis-dimethylamino tin and peroxide for transparent flexible electronics. Appl Surf Sci 313:585–590
19. Bisquert J, Cendula P, Bertoluzzi L, Gimenez S (2014) Energy diagram of semiconductor/electrolyte junctions. J Phys Chem Lett 5:205–207
20. Xia Z, Rozyyev V, Mane AU, Elam JW, Darling SB (2021) Surface zeta potential of ALD-grown metal-oxide films. Langmuir 37:11618–11624
21. Kavan L (2014) Lithium insertion into TiO_2, (anatase): electrochemistry, Raman spectroscopy, and isotope labeling. J Solid State Electrochem 18:2297–2306
22. Beerbom MM, Lägel B, Cascio AJ, Doran BV, Schlaf R (2006) Direct comparison of photoemission spectroscopy and in situ Kelvin probe work function measurements on indium tin oxide films. J Electron Spectr Rel Phen 152:12–17
23. Michaelson HB (1977) The work function of the elements and its periodicity. J Appl Phys 48:4729–4733
24. Hsu CH, Mansfeld F (2001) Technical note: concerning the conversion of the constant phase element parameter Y0 into a capacitance. Corrosion 57:747–748
25. Hengerer R, Kavan L, Krtil P, Grätzel M (2000) Orientation dependence of charge transfer processes on TiO_2, (anatase) single crystal. J Electrochem Soc 147:1467–1472
26. Bolts JM, Wrighton MS (1976) Correlation of photocurrent-voltage curves with flat-band potential. J Phys Chem 80:2641–2645
27. King LA, Yang Q, Grossett ML, Galazka Z, Uecker R, Parkinson BA (2016) Photosensitization of natural and synthetic SnO_2 single crystals with dyes and quantum dots. J Phys Chem C 120:15735–15742

28. Baena JPC, Steier L, Tress W, Saliba M, Neutzner S, Matsui T, Giordano F, Jacobsson TJ, Kandada ARS, Zakeeruddin SM, Petrozza A, Abate A, Nazeeruddin MK, Grätzel M, Hagfeldt A (2015) Highly efficient planar perovskite solar cells through band alignment engineering. Energy Environ Sci 8:2928–2934
29. Hu T, Becker T, Pourdavoud N, Zhao J, Brinkmann KO, Heiderhoff R, Gahlmann T, Huang Z, Olthof S, Meerholz K, Tobbens D, Cheng B, Chen Y, Riedl T (2017) Indium-free perovskite solar cells enabled by impermeable tin-oxide electron extraction layers. Adv Mater 29:1606656
30. Erdenebileg E, Wang H, Li J, Singh N, Dewi HA, Tiwari N, Mathews N, Mhaisalkar S, Bruno A (2021) Low-temperature atomic layer deposited electron transport layers for co-evaporated perovskite solar cells. Solar RRL 6:2100842